Numerical investigation of the impact of injectors location on fuel mixing in the HIFiRE 2 Scramjet combustor

Authors

Sasi Kiran Palateerdham [1], Lakshmi Narayana Phaneendra Peri [2], Antonella Ingenito [3], Ashish Vashishtha [4]*

* Corresponding author

[1] PhD student, School of Aerospace Engineering, Sapienza University of Rome, Italy, sasikiran.palateerdham@uniroma1.it

[2] Research Fellow, School of Aerospace Engineering, Sapienza University of Rome, Italy, phanindra.p123@gmail.com

[3] Professor, School of Aerospace Engineering, Sapienza University of Rome, Italy, Antonella.ingenito@uniroma1.it

[4] Lecturer, South East Technological University, Carlow Campus, Ireland, ashish.vashishtha@setu.ie

ABSTRACT

In scramjets, the position and direction of the injectors plays a crucial role for fuel/air mixing and combustion efficiency. Fuel injection is still a potential topic of research to be addressed, in fact an effective fuel injection strategy is critical for increasing the streamwise vorticity that has been found to be the main responsible for the fuel-air mixing in compressible flows. In fact, the position and the direction of the fuel injectors, the presence of a cavity scramjet has a critical influence on the density and pressure gradients, and consequently on the baroclinic term that is a source of vorticity. In this regard, this research wants to investigate the nature of the mixing in supersonic flows, investigating the contribution between the streamwise and stretching component for the vorticity. Numerical modelling of supersonic combustion using Large Eddy Simulations was carried out in HIFiRE 2 Scramjet to better understand the physics of the combustion and mixing.

Nomenclature

C_p	Specific heat capacity at constant pressure (J/Kg. K)
D	Scalar diffusion coefficient (m^2s^{-1})
d	Injector diameter (m)
E	Total specific energy (J/kg)
e	Specific internal energy (J/kg)
h	Specific enthalpy (J/kg)
k	Turbulent kinetic energy
Le	Lewis number
Ma	Mach number
N	Number of species
Pr	Prandtl number
p	Pressure (Pa)
q_i	Heat flux ($J/m^2.s$)
S	Source-term vector
Sc	Schmidt number
t	Time variable
T	Temperature (k)
U	Vector of conserved variables
u_j	Velocity (m/s)
U	Inflow velocity (m/s)
$\tilde{U}$	Total filtered
V	Cartesian velocity vector
W	Species molecular weight
X	Cartesian position vector

Y	Species mass fraction
y	wall-normal direction
Z	Mixture fraction
Dn	nth-species diffusion coefficient,
Wn	nth-species molecular weight,
Yn	mass fraction,
Vn	Diffusing at velocity
Jn	diffusive mass flux
Di	molecular diffusion coefficient, of species i
n	time step

INTRODUCTION:

Scramjet and Ramjet engines are the current interest of research for many nations and research agencies for their national defense, for future green aviation missions [1]. Reliability of these fast-moving vehicles depends on the combustion stability during high altitude flight conditions as the ignition and flame anchoring area complex processes depending on chemical reactivity, species transportation rate, flow conditions, residual time, geometry of the combustor [2].

Due to the high velocities involved, combustion stability is a key challenge in dual-mode combustors. At moderate M_{flight} the incoming air temperature could be inadequate to ensure the flame holding, therefore a region with a favourable equivalency ratio, temperature, pressure, and velocity where the reaction are stable and serve as a source of heat and radicals to the remaining fuel-air combination is critical. In contrast, at extremely high M_{flight}, the incoming air temperature is high enough that the auto-ignition delay time is minimal. The combustion stability problem is reduced to a mixing problem in this auto-ignition regime [3].

The residence time in these engines is of the order of fractions of millisecond. In such a short time, injected fuel must accomplish efficient mixing with the incoming supersonic air to facilitating flame anchoring. In the supersonic combustion, a vast range of phenomena can occur, which results from interactions between injector flows, shock waves, boundary layers, and cavity flow. The combustion efficiency in scramjet combustor is highly sensitive that even minor losses owing to ineffective combustion, coupled with large friction losses, boundary layer/shock wave interactions, and overall total pressure losses, might result in low or even negative engine efficiency. Assuring a good ignition and flame stability while avoiding excessive total pressure losses has long been one of the goals of scramjet combustion research. [4-8].

Fuel Mixing Improvement in Supersonic Flows

In order to understand how to improve the fuel mixing, , the dimensionless vorticity equation for compressible flows is introduced:

$$\frac{\partial \bar{\omega}}{\partial t}+\left(\bar{u}\cdot\bar{\nabla}\right)\bar{\omega}=\bar{\omega}\cdot\overline{\overline{\nabla u}}-\bar{\omega}\left(\bar{\nabla}\cdot\bar{u}\right)+\frac{\overline{\nabla\rho}\times\overline{\nabla p}}{\rho^2}+\frac{1}{\mathrm{Re}}\nu\overline{\overline{\nabla^2\omega}}+\frac{1}{\mathrm{Re}}\left(-\frac{1}{\rho^2}\overline{\nabla\rho}\times\left(\bar{\nabla}\cdot\bar{\bar{\sigma}}\right)+\frac{1}{\rho}\left\{\overline{\nabla\mu}\times\left[\overline{\nabla^2 u}+\bar{\nabla}\left(\bar{\nabla}\cdot\bar{u}\right)\right]+2\bar{\nabla}\times\left(\bar{\bar{E}}\,\overline{\nabla\mu}\right)\right\}\right)$$

The vorticity equation, except for the baroclinic term and the effects due to the variation of molecular properties (due for example to combustion) is a homogeneous equation in w. The first term of the

equation represents the vorticity change due to the non-stationarity of the field, while the second term represents its convective transport.

From this equation it can be deduced that in supersonic flows the convective term, that of vortex stretching (the 3rd), that of compression (the 4th) and the baroclinic (the 5th) have the same order of magnitude and therefore the same influence on the flow both at large and small scales. The viscous terms are multiplied by the inverse of the Reynolds number and therefore at large scale are negligible.

The term vortex stretching represents the effect of average motion on turbulence. In addition, decomposing the stress tensor into its symmetric and antisymmetric part yields:

$$\bar{\omega}\cdot\overline{\overline{\nabla u}} = \bar{\omega}\cdot Sym\overline{\overline{\nabla u}} + \bar{\omega}\cdot Skw\overline{\overline{\nabla u}}$$

being $\bar{\omega}\cdot Skw\overline{\overline{\nabla u}} = 0$, it follows:

$$\bar{\omega}\cdot\overline{\overline{\nabla u}} = \bar{\omega}\cdot Sym\overline{\overline{\nabla u}}$$

From this equation it can be deduced that the term vortex stretching represents the speed with which a volume is deformed due to the effect of velocity gradients. Considering, for example, swirling tubes, we have that due to vortex stretching these are stretched triggering a process of generation of smaller and smaller vortices. For the conservation of angular momentum, as the size of the vortices decreases there is an increase in their rotation speed and therefore an increase in the fluctuations observed in the field.

The term $\bar{\omega}\left(\bar{\nabla}\cdot\bar{u}\right)$ It is present only in compressible flows: this term has the effect of concentrating or dispersing the vorticity present in the field depending on whether there are local compressions or expansions. The term baroclinic $\frac{\overline{\nabla\rho}\times\overline{\nabla p}}{\rho^2}$ Indicates the creation of vorticity due to the presence of pressure and density gradients. The presence of a pressure field and density inhomogeneity (caused, for example, by the different densities of the two currents), in fact, gives greater acceleration to areas with lower density: this effect (baroclinic) can be a source or well for vorticity. The other terms show the effect of viscous dissipation which is mainly to dissipate the energy of vortices by destroying vortex structures; However, it must be borne in mind that, in some cases, such terms can be sources for vorticity.

The increase in temperature due to combustion, however, has the effect of expanding the flow and therefore tends to relaminate it. At the same time, however, since at Ma>1 the fluctuations in velocity due to combustion give rise to local compressions and therefore to an increase in vorticity in the flow, temperature plays two opposite roles on vorticity. Moreover, since the Mach number does not appear in its equation, if there is vorticity in the flow its transport is independent of the absolute velocity even if its presence is linked more than to the velocity itself, to the speed gradients (at high Mach having gradients is not simple.

Theoretical works by several authors [4, 5] have shown that mixing can be accelerated by increasing streamwise vorticity. This can be obtained by favouring the formation of pressure and density gradients, e.g., by means of different injector designs, such as transverse, swirl, strut, wall or swept ramp injectors, and by means of a proper location.

In this context, the analysis of the helicity, H:

$$H = \bar{\omega} \cdot \bar{u}$$

may help to understand how to improve the stremwise vorticity. In fact, when the helicity is maximum, the mixing transport from large to small scales is mainly affected by the steamwise vorticity.

In order to verify the balance between the rotation rate $\Omega^2=\Omega ij\Omega ij$ ($\Omega ij=(ui,j-uj,i)/2$) and the strain rate $S^2=SijSij$, ($Sij=(ui,j+uj,i)/2$), where Ω and S are respectively the antisymmetric and the symmetric components of ∇u, the Q criterion has been introduced.

In fact, the Q criterion states that positive Q isosurfaces indicate areas where the streamwise vorticity overcomes the spanwise component, thus making those surfaces eligible as vortex initial structures. This means that by looking at the temporal evolution of these iso-surfaces, it could be possible to visualize the vortices development and if the deformation of a fluid element is mainly related to strength of rotation or the strain that directly affects the stretching of the vortex tube in subsonic flows.

Description of the Computational Domain

The combustor test section is illustrated schematically in Fig. 1. The flow direction is configured to be positive x. The total length of the combustor is 711.3 mm including the isolator, cavity and the combustion chamber. There is symmetric arrangement of injectors in array on the top and bottom of the combustor walls. Four primary injectors with a diameter of 3.18 mm and an inclination of 15º, are located at 244 mm from the inlet. Four secondary injectors with a diameter of 2.39 mm and an inclination angle normal to the combustion chamber wall are located at 419 mm downstream of the isolator entry. The cavity is located downstream of the primary injectors. The combustor's throat height is set at 25.4 mm and maintained till a distance of 203.2 mm after divergence in the isolator's cross-section is noticed with an included angle of 2.6º. The cavity flame holder begins at 294.5 mm downstream of the isolator entrance and continues until the close-out ramp converges with the 2.6 deg inclined wall surface at 401.2 mm.

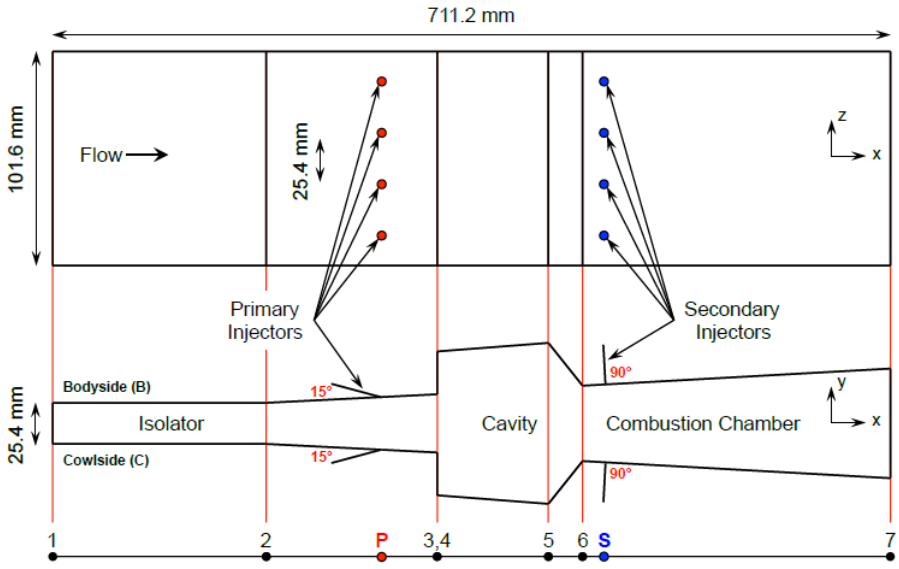

Fig 1. Schematic diagram of HIFiRE 2 Scramjet. Image credit [7]

A three-dimensional unstructured grid of 4.6 million nodes was constructed by means of the ANSYS Work bench (see Fig.2).

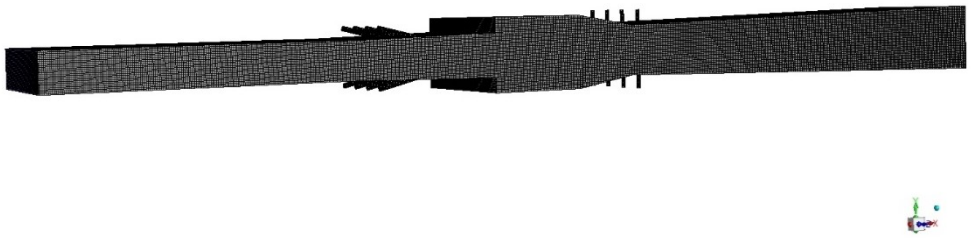

Fig 2. HiFIRE 2 Mesh

GOVERNING EQUATIONS

In Numerical Modelling, the balance governing equations for the LES for conservation of mass, momentum, energy and species transport are expressed as:

Equation of Mass Conservation

$$\frac{\partial \bar{\rho}}{\partial t} + \frac{\partial \bar{\rho}\widetilde{u_i}}{\partial x_i} = 0 \qquad \text{Eq. 1}$$

Transport Equation of Momentum

$$\frac{\partial(\bar{\rho}\widetilde{u_j})}{\partial t} + \frac{\partial(\bar{\rho}\widetilde{u_i}\widetilde{u_j} + \bar{p}\delta_{ij})}{\partial x_i} = \frac{\partial \tilde{\tau}_{ij}}{\partial x_i} + \frac{\partial \tau_{ij}^{sgs}}{\partial x_i} \qquad \text{Eq. 2}$$

Transport Equation of Total Energy (internal + mechanical)

$$\frac{\partial(\bar{\rho}\widetilde{U})}{\partial t} + \frac{\partial(\bar{\rho}\widetilde{u_i}\widetilde{U} + \bar{p}\widetilde{u_i} + \bar{q_i} - \widetilde{u_i}\overline{\tau_{ij}} + H_i^{sgs} - \sigma_i^{sgs})}{\partial x_i} = 0 \qquad \text{Eq.3}$$

Transport Equations for the Ns species mass fractions

$$\frac{\partial(\bar{\rho}\tilde{Y}_n)}{\partial t} + \frac{\partial(\bar{\rho}\tilde{u}_j\tilde{Y}_n)}{\partial x_i} = \frac{\partial}{\partial x_i}\left[\bar{\rho}(D_n + D_{t,n})\frac{\partial\tilde{Y}_n}{\partial x_i}\right] + \bar{\rho}\widetilde{\dot{\omega}_n} \qquad \text{Eq. 4}$$

Thermodynamic Equation of State

$$\bar{p} = \bar{\rho}\sum_{i=1}^{N_s}\frac{\tilde{Y}_i}{W_i}\mathcal{R}_u\tilde{T} \qquad \text{Eq.5}$$

These equations must be coupled with the constitutive equations which describe the molecular transport. In the above equations, *t* is the time variable, ρ the density, *uj* the velocities, t_{ij} the viscous stress tensor, and $\tilde{U}$ the total filtered energy per unit of mass, that is sum of the filtered internal energy, $\tilde{e}$, the resolved kinetic energy, $1/2(\widetilde{u_i u_i} - \tilde{u}_i\tilde{u}_i)$, and the subgrid one, $1/2(\widetilde{u_i u_i} - \tilde{u}_i\tilde{u}_i)$, *qi* is the heat flux, *p* the pressure, *T* the temperature.

The stress tensor and the heat-flux are respectively:

$$\overline{\tau_{ij}} = 2\mu(\widetilde{S_{ij}} - \frac{1}{3}\widetilde{S_{kk}}\delta_{ij}) \qquad \text{Eq. 6}$$

$$\bar{q}_i = -k\frac{\partial(\tilde{T})}{\partial x_i} + \bar{\rho}\sum_{n=1}^{N_s}\widetilde{h_n}\widetilde{Y_n}\widetilde{V_{i,n}} + \sum_{n=1}^{N_s}q_{i,n}^{sgs} \qquad \text{Eq. 7}$$

Dn is the n[th]-species diffusion coefficient, *Wn* the n[th] species molecular weight, *Yn* the mass fraction, w_n is the production/destruction rate of species *n*, diffusing at velocity $V_{i,n}$ and resulting in a diffusive mass flux *Jn*. Finally, *Ru* is the universal gas constant. Summation of all species transport equations yields the total mass conservation equation. Therefore, the *Ns* species transport equations and the mass conservation equation are linearly dependent and one of them is redundant. Furthermore, to be consistent with mass conservation, the diffusion fluxes ($\boldsymbol{J_n = \rho Y_n V_n}$) and chemical source terms must satisfy:

$$\sum_{n=1}^{N_s} J_n = 0 \quad \text{and} \quad \sum_{n=1}^{N_s}\dot{\omega}_n = 0 \qquad \text{Eq.8}$$

In particular, the constraint on the summation of chemical source terms derives from mass conservation for each of the *Ns* chemical reactions of a chemical mechanism.
The sub grid scales are modelled using Smagorinsky-Lilly model. The eddy viscosity being modelled as $\nu_t = C\Delta^2\sqrt{2\bar{S}_{ij}\bar{S}_{ij}} = C\Delta^2|\bar{S}|$. Here Δ is the size of the grid and C is the constant.

Boundary Conditions

Table 1 shows the boundary conditions at the intake and exit of the combustor. The air and fuel inlet conditions correlate to a dual-mode operation. The supersonic air enters the isolator at Mach 3.46, and the fuel is injected at sonic speeds through the primary and secondary injectors. The fuel injected is JP7, which has been based on a combination of 36% methane and 64% ethylene. A global 3-step reaction mechanism is implemented involving the combustion of methane, ethylene and the formation of carbon dioxide, carbon oxide and water. The current model is taken from Guilhem Lacaze et al.[7]. Arrhenius parameters are shown in Table 2.

Table 1. Inflow Boundary Condition parameters

Inflow Boundary	Pressure [KPa]	Temperature [K]	Mach
Isolator	40.3	736.2	3.46
Primary Injector	105.7	293.3	1.0
Secondary Injector	290.7	301.1	1.0

$$CH_4 + 1.5O_2 + M \Rightarrow CO + 2H_2O + M \qquad (R1)$$

$C_2H_4 + 2O_2 + M$ => $2CO + 2H_2O + M$ (R2)

$2CO + O_2 + M$ <=> $2CO_2 + M$ (R3)

Table 2. Arrhenius parameters for the chemical mechanism

	A [cgs]	**β [-]**	**E_a [cal/mol]**
R1	$2.0e^{15}$	0.0	$35.0e^{3}$
		v^f_{CH4}=0.9, $v^f_{O2} = 1.1$	
R2	$4.9e^{9}$	0.0	$35.5e^{3}$
		v^f_{C2H4}=0.5, $v^f_{O2} = 0.65$	
R3	$2.0e^{9}$	0.0	$12.0e^{3}$
		v^f_{CH4}=0.9, $v^f_{O2} = 1.1$ $v^f_{O2} = 1.1$	

NUMERICAL MODELLING

The scramjet combustor numerical modeling was carried out utilizing a density-based double precision solver in combination with a 3D compressible LES (Large Eddies Simulations) equation using ANSYS FLUENT. For numerical analysis of the flow field with turbulence using conventional constants, the Large Eddy Simulation (LES) model is used. WALE subgrid scale model was used to produce a precise solution with steady convergence characteristics to represent the effects of unresolved small-scale fluid motions (such as small eddies, swirls, vortices) in the equations governing the large-scale motions that are resolved in computer model. By choosing a Courant Friedrichs Levy value of 0.3 standard acceptable stability can be is ensured (Pandey and Choubey, 2017). The pressure outlet boundary condition is defined at the computational domain. Due to the supersonic flow, all physical variables are extrapolated from the interior cells..Non-reflective boundary conditions have been implemented.

To resolve the flow field in the scramjet combustor, a three-dimensional unstructured grid was constructed in ANSYS Work bench using adaptive method. To achieve precise results, a fine mesh was adopted to carry out the numerical analysis. The number of nodes is evaluated to be around 4.6 million.

NUMERICAL RESULTS

In this paper, a comparison between different times has been made, starting from the ignition to the stationarity conditions of the flow. Figure 3 shows the top view of the pressure contour at a distance from the wall od 0.01 m from the upper wall. Statistics from the LES are obtained by time-averaging instantaneous flow-fields after 3 flow-through times.

Due to the interaction of the incoming supersonic air flow with the 4 fuel injectors inclined with respect to the airflow of 15°, a bow shocks arises increasing the pressure from 40300 Pa to 85000 Pa (see Fig. 4, 5 6). Shock waves reflect from the upper and lower wall, increasing the averaged pressure through the combustor until 48 kPa. From this point due to the sudden increase in area due to the cavity, the pressure decreases to 43 kPa, but this decrease is mitigated by the release of heat and the pressure starts increasing again 94 kPa.

It is explained by means of the Raleigh law that states that the addition of heat to a supersonic flows increases the pressure. In corresponding to the secondary injectors, the pressure reaches its maximum of 210, 225 and 250 kPa for the three different timesteps. From this point forward, the pressure starts decreasing to 98 kPa due to the divergent angle of the combustor. The flow due to the release of heat reaches the condition of thermal chocking. Because of the transverse injection of the secondary injectors, the pressure suddenly increases reaching its maximum of 222 kPa. From this point the pressure decreases due to the divergent section of the combustor.

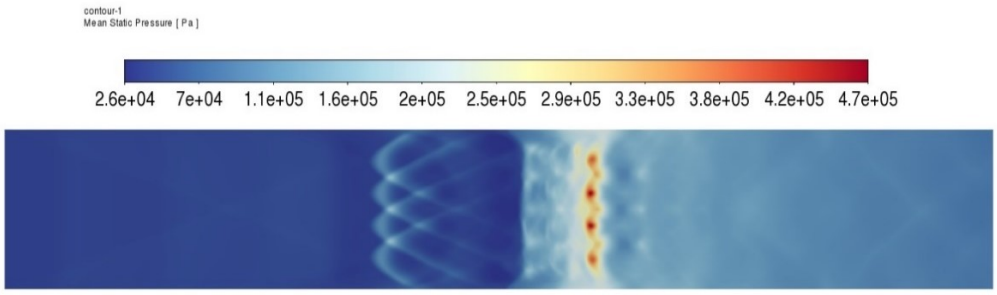

Figure 3. Mean Pressure at the wall-parallel plane Y=0.01 m

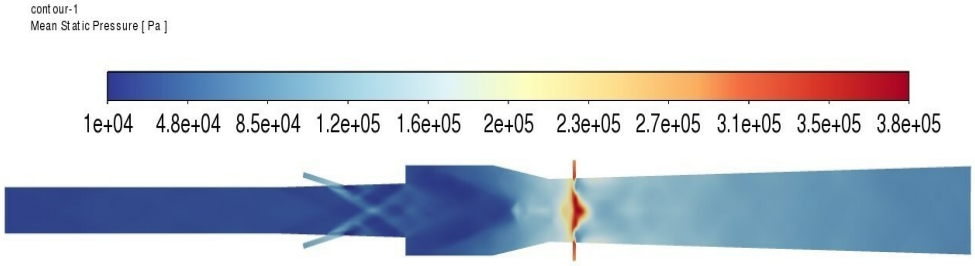

Figure 4. Mean Pressure on the transverse planes passing through the center of the injectors.

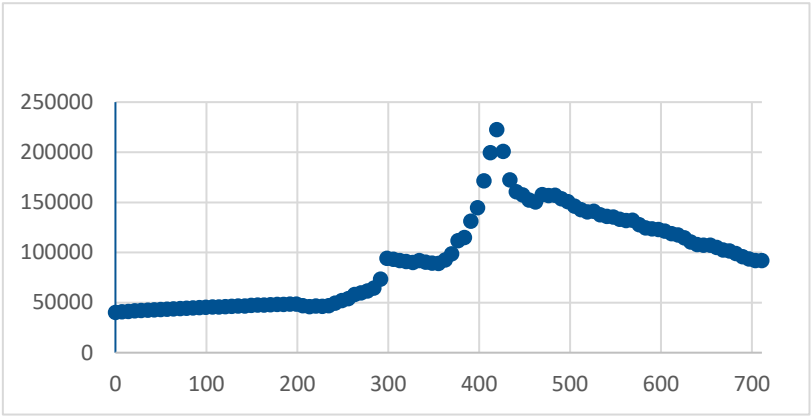

Figure 5. Instantaneous pressure distribution along the axial length at t=0.02 s

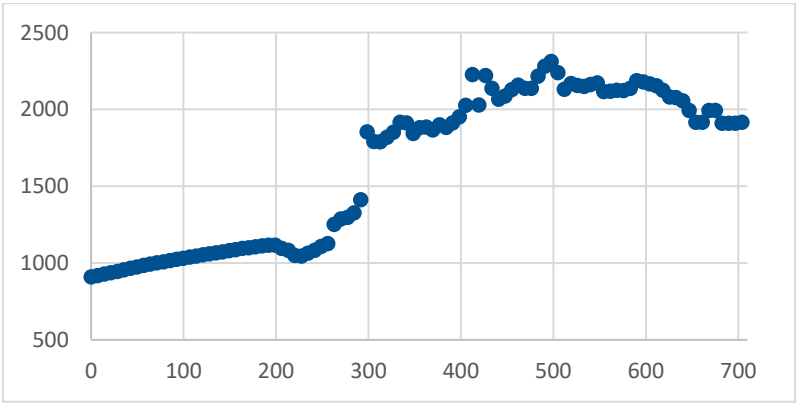

Figure 6 Instantaneous temperature distribution along the axial length at t=0.02 s

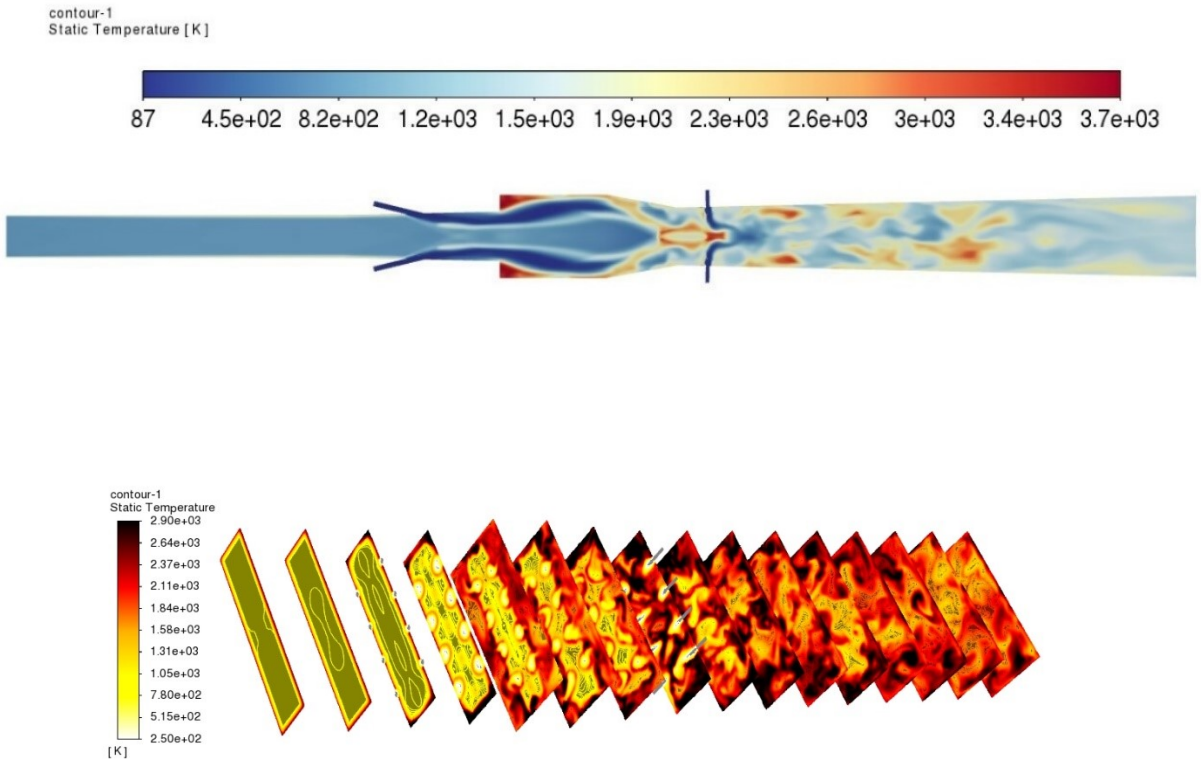

Figure 7. Instantaneous Temperature on the transverse planes passing through the center of the injectors (up) and in the axial direction bottom.

Fig. 6 shows that the temperature increases to 1117 K until the primary injection: there due to the mixing with the JP4 injection, slightly decreases to 1064 K. From this point starts again increasing, reaching its maximum of 2300 K. The temperature then keeps almost constant, nevertheless the divergence of the combustion, due to the heat release due to the combustion, as confirmed from the H2O mass fraction trend (see Fig. 7).

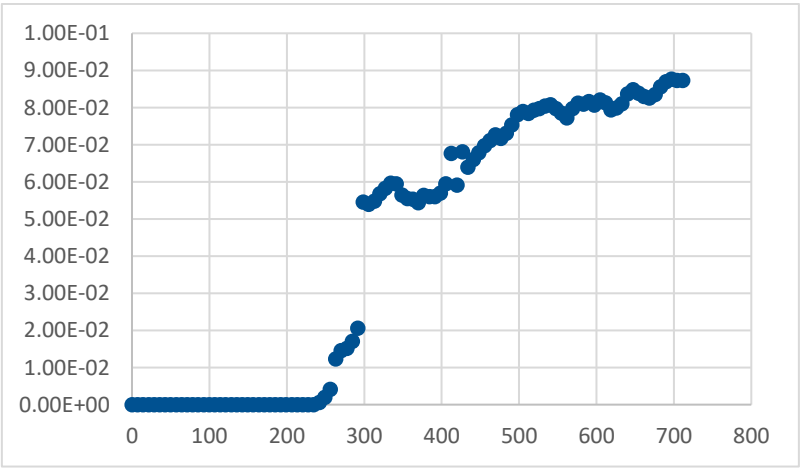

Figure 9 Instantaneous H2O distribution along the axial length at t=0.02 s

Fig. 8 and Fig. 9 show that the Mach number starts decreasing due to the oblique shock waves arising through the combustor until Mach 2.9. Downstream of the primary injection, due to the heat release, the Mach number

keep decreasing sharply due to the heat addition. In correspondence to the cross flow secondary injection, the Mach number reaches the sonic condition.

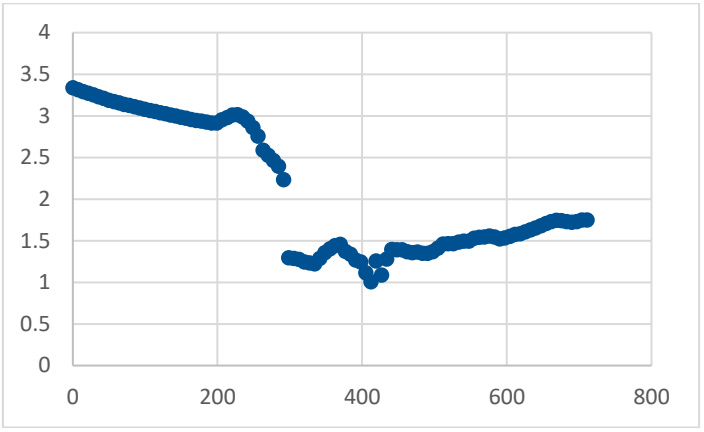

Figure 10 Instantaneous Mach distribution along the axial length at t=0.02 s

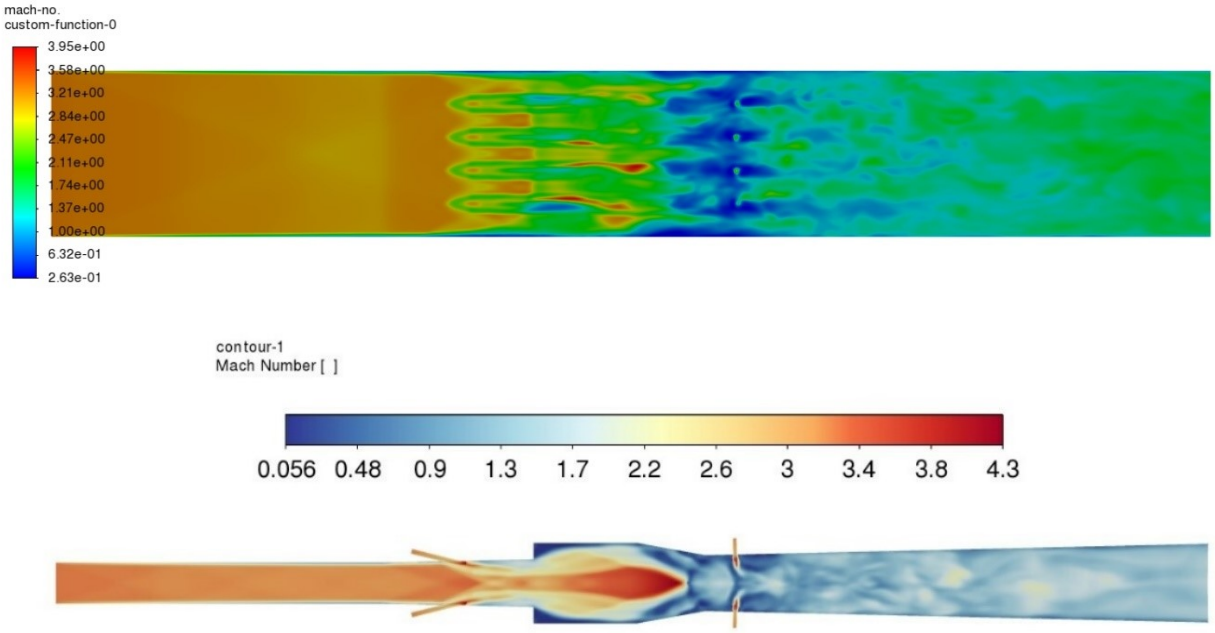

Figure 11 Average Mach flow field at Y=0,01 (top), Instantaneous Mach in the trasversal plane passing through the center of the injectors (bottom) .

In fact, in a supersonic flow, the addition of heat (T0/T*) causes a decrease in the Mach number, as shown in Fig. 10. The divergent part of the combustor allows the Mach number to increase and establish again the supersonic conditions and reaching M=1.75.

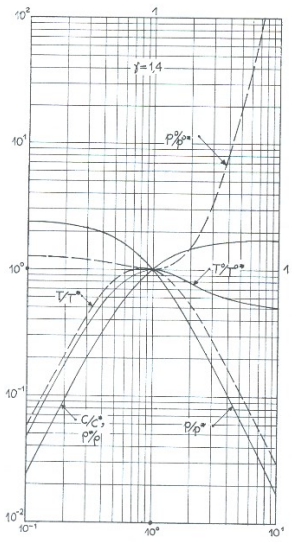

Figure 12. thermodynamic property ratios as a function of Mach number using the Raleigh flow model.

Figure 11 and 12 show the instantaneous contour of the C2H4 and H2O mass fraction at t=0.0024. These figures show then the flame start anchoring upstream of the fuel injection and the primary fuel is almost completely burned into the cavity. The secondary fuel injection, responsible for the high pressure increase due to the bow shock and for the flame ignition, burns efficiently in the second part of the combustor.

The efficiency of combustion computed is about 97%, calculated considering the unburned mass at the outlet with respect to the injected mass.

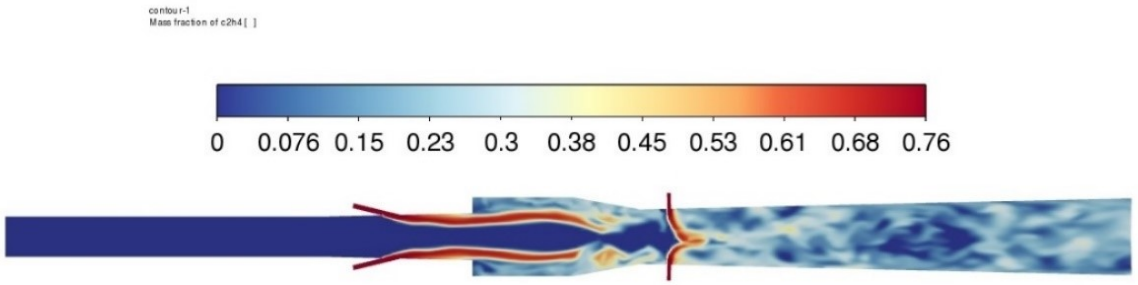

Figure 13 Instantaneous C2H4 in the trasversal plane passing through the center of the injectors

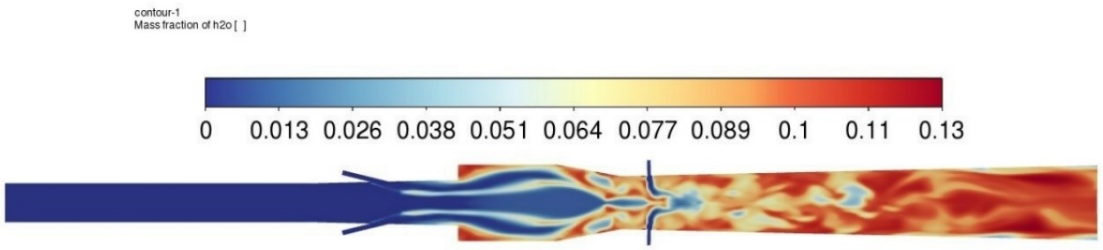

Figure 14 Instantaneous H2O in the trasversal plane passing through the center of the injectors

Fig 13 shows the vorticity field within the combustor. At the entrance of the combustor the vorticity is practically nil. In the interface regione between the air and the primary injectors, the vorticity increases up to 470000 Hz. This increase in vorticity is due, as previously mentioned, to the term baroclinic, which is a source of vorticity in supersonic flows. This means that mixing times are of the order of 10-5 10-6 s, i.e. almost two order of magnitude less then the residence time. The vorticity also contribute to the mixing and combustion within the cavity. The helicity increases from almost 0 to $3x10^8$, confirming the vorticity deformation is mainly due to the streamwise component, that very quickly mix fuel and oxidizer.

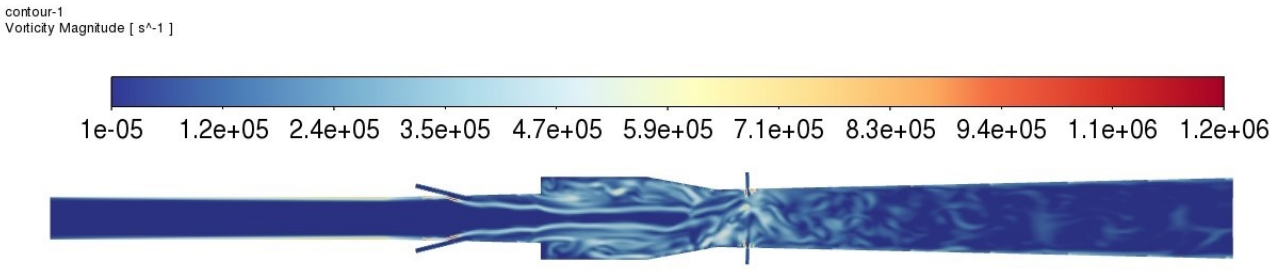

Figure 15 Instantaneous vorticity in the trasversal plane passing through the center of the injectors

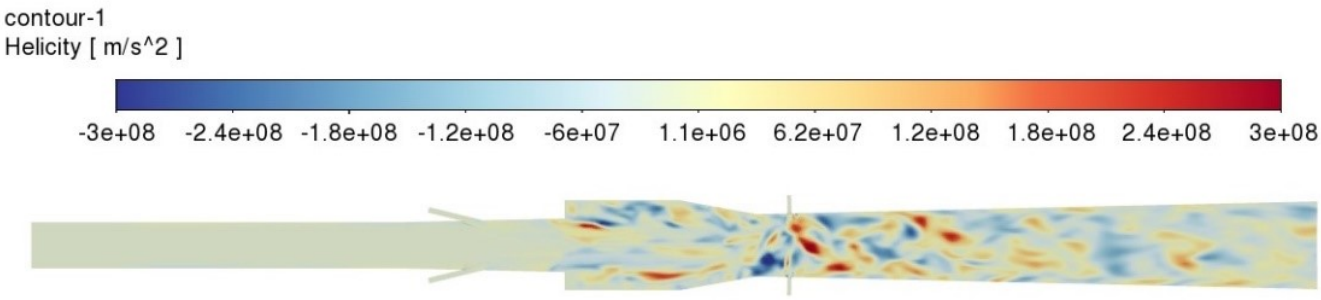

Figure 16 Instantaneous helicity in the trasversal plane passing through the center of the injectors

Figure 15 shows the vortex structures arising from the primary injection, responsible for the fuel/air mixing and combustion. This result confirm that the cavity downstream of the inclined injection, coupled with the cross flow secondary injection is able to ensure a good mixing and combustion efficiency.

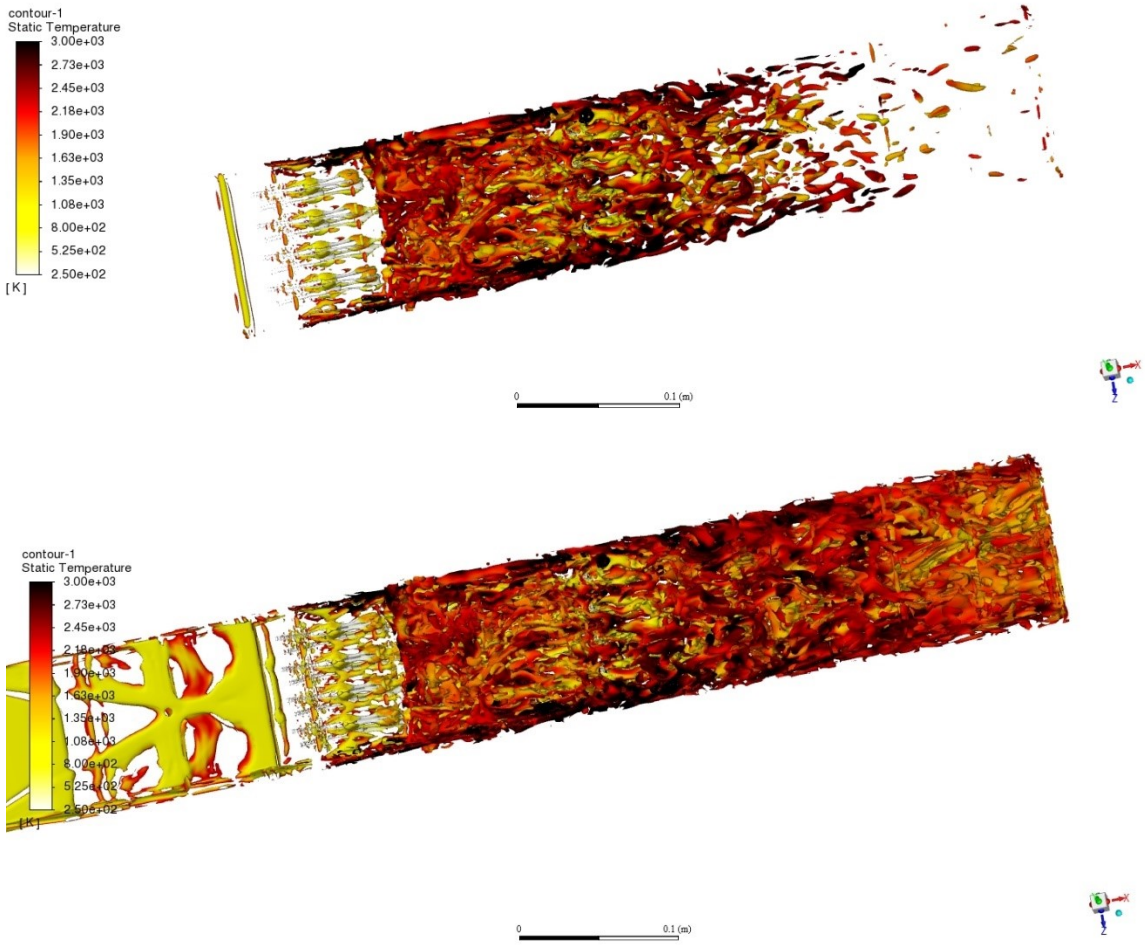

Figure 17 Q=0.1 and Q=100 Isosurface coloured by Instantaneous temperature

CONCLUSION

In this paper large eddies Simulations have been performed to investigate mixing and combustion in supersonic flows. The Q criterion has shown that the deformation of the vortex structures is mainly related to the streamwise vorticity. Mixing times have been estimated of the order of 10-5 10-6 s, i.e. almost two order of magnitude shorter than the residence time. Due to this efficient mixing, the combustion efficiency, for the boundary conditions considered is about 97%.

References

[1] Qili Liu, Damiano Baccarella, Will Landsberg, A. Veeraragavan, Tonghun Lee, "Cavity flame holding in an optical axisymmetric scramjet in Mach 4.5 flows" Proceedings of the Combustion Institute 37, Issue 3, 2019, Pages 3733-3740

[2] Robert D. Stachler, Joseph K. Lefkowitz, Joshua S. Heyne, Scott D. Stouffer, Timothy M. Ombrello , Joseph D. Miller, "The impact of residence time on ignitability and time to ignition in a toroidal jet-stirred reactor" Proceedings of the Combustion Institute 37 (2019) 5039–5046

[3] Daniel J. Micka *, James F. Driscoll, "Combustion characteristics of a dual-mode scramjet combustor with cavity flame holder", Proceedings of the Combustion Institute 32 (2009) 2397–2404

[4] A. Ingenito · D. Cecere · E. Giacomazzi, “Large Eddy simulation of turbulent hydrogen-fueled supersonic combustion in an air crossflow” shock waves, volume 23, pages 481-494 (2013)

[5] Qili Liu, Damiano Baccarella, Tonghun Lee, Review of combustion stabilization for hypersonic airbreathing propulsion, https://doi.org/10.1016/j.paerosci.2020.100636

[6] R.J. Yentsch, D.V. Gaitonde, Numerical investigation of dual-mode operation in a rectangular scramjet flowpath, J. Propuls. Power. 30 (2014) 474–489, https://doi.org/10.2514/1.B34994

[7] R.J. Yentsch, D.V. Gaitonde, Unsteady three-dimensional mode transition phenomena in a scramjet flowpath, J. Propuls. Power. 31 (2015) 104–122, https://doi.org/10.2514/1.B35205.

[8] A. Saghafian, L. Shunn, D.A. Philips, F. Ham, Large eddy simulations of the HIFiRE scramjet using a compressible flamelet/progress variable approach, Proc. Combust. Inst. 35 (2015) 2163–2172, https://doi.org/10.1016/j. proci.2014.10.004.

[9] Yves Dubief, and Franck Delcayre, JOURNAL OF TURBULENCE 2000.